ARTICLE OPEN

Check for updates

In-situ self-crosslinking strategy for autonomous self-healing materials

Yan Song[1], Annan Kong[1], Dongxiang Chen[1] and Guo Liang Li[1]✉

Autonomous self-healing anticorrosion protective coatings from intrinsic polymers is a great challenge. In this work, in-situ self-crosslinking strategy was demonstrated for constructing self-healing anticorrosion polymers. The as-synthesized polymers had tunable catechol content and mechanical properties. The specimens could be repaired in an Fe^{3+} solution owing to the formation of dynamic catechol-Fe^{3+} coordination crosslinking sites. Moreover, when scratched, the prepared polymers exhibited a self-healing anticorrosion performance, as evidenced by salt immersion and electrochemical impedance spectroscopy. An in-situ self-crosslinking mechanism was proposed, which was derived from the dynamic coordination of catechol groups in the polymer chains and Fe^{3+} produced from the metal substrate. This intrinsic self-healing anticorrosion polymer are highly potential for anticorrosion applications in harsh environments.

npj Materials Degradation (2023)7:67 ; https://doi.org/10.1038/s41529-023-00381-2

INTRODUCTION

Self-healing materials inspired by living tissues have attracted considerable attention owing to their prolonged lifetime, enhanced reliability, and durability[1–3], and have been employed in many fields, such as anticorrosion coatings[4–6]. In contrast to conventional coatings, self-healing anticorrosion coatings can repair damage and recover their anticorrosion function[7]. Their main function is the autonomous protection of the metal surface from corrosion via reconstruction of the barrier or release of corrosion inhibitors to passivate defects in the metal substrates[8–10]. This strategy does not involve any human intervention, which is critical for the long-term performance of metallic materials in corrosive environments.

Self-healing anticorrosion coatings generally utilize the extrinsic strategy of imbedding microcapsules or nanocontainers containing self-healing agents or corrosion inhibitors[4,11]. In the microcapsule systems, healing agents—such as tung oil[12], silyl ester[13] and isophorone diisocyanate[14]—encapsulated by a polymer shell —such as polyurethane/poly(urea-formaldehyde)[15]—are released and polymerized to form a protective layer and seal the scratch. For nanocontainer systems, corrosion inhibitors have been preloaded in halloysite nanotubes[16–18], mesoporous silica nanoparticles[19,20], zeolitic imidazolate framework[21,22], polymer microspheres[23,24] or nanofibers[25]. Upon the onset of corrosion triggered by the mechanical pressure, pH modification, light irradiation, etc., the corrosion inhibitors are released into the defect areas and autonomously protect the metal surface[26]. Recently, an improvement in self-healing anticorrosion coatings was related to the efficient release of corrosion inhibitors and the formation of a durable protective film that seals the damaged area by constructing composites[27–32]. Since incorporating additives into coatings generally compromises their integrity and destructs their barrier and mechanical properties[7], the intrinsic self-healing process relies on the recombination of dynamic interactions, which makes the use of additives unnecessary. Non-covalent (such as hydrogen bonds[33,34], metal-ligand coordination bonds[35], host-guest interactions[36], and ionic bonds[37]) or covalent bonds (such as disulfide bond[38], Diels-Alder reaction[39], and transesterification reaction[40]) are utilized to construct intrinsic self-healing polymer coatings. However, external intervention, such as heating, is generally required for intrinsic self-healing to proceed[41,42], which poses a challenge to the development of an autonomous self-healing anticorrosion coating using intrinsic polymers that can restore anticorrosion properties without human intervention.

Herein, in-situ self-crosslinking strategy of intrinsic polymers for preparing autonomous self-healing anticorrosion coating is proposed. When the prepared polymers was damaged, the metal substrate corroded and generated Fe^{3+}. Subsequently, dynamic metal coordination crosslinks were formed between the Fe^{3+} and catechol groups in the polymer chain, thus restoring the anticorrosion properties of the coating. Compared to extrinsic self-healing anticorrosion coatings, the intrinsic polymer coating in this study was capable of restoring anticorrosion performance without any additives or external human intervention.

RESULTS AND DISCUSSION

Synthesis and characterization of intrinsic self-healing anticorrosion polymers (ISAP)

Previous self-healing anticorrosion coatings consist of a polymer matrix and embedded self-healing microcapsules. When the coating is damaged, the released self-healing agents or corrosion inhibitors from capsules accumulate at the breakage and inhibit corrosion. Supplementary Fig. 1 illustrates the ISAP coating in this work. The designed ISAP repairs the breakage through the crosslinking of catechol in the polymer chain with Fe^{3+} produced from the damaged region of the metal. The molecular structure and synthesis process of the ISAP are shown in Fig. 1 and Supplementary Fig. 2. A catechol-containing chain extender was synthesized and characterized. Its chemical structure was confirmed using ^{1}H NMR and ^{13}C NMR spectroscopy (Supplementary Figs. 3 and 4)[43]. The polymer was synthesized using α,ω-aminopropyl-terminated poly(-dimethylsiloxane) (PDMS), isophorone diisocyanate (IPDI) and the synthesized chain extender (Supplementary Fig. 2).

[1]State Key Laboratory of Chemical Resource Engineering, College of Materials Science and Engineering, Beijing University of Chemical Technology, Beijing 100029, China. ✉email: glli@buct.edu.cn

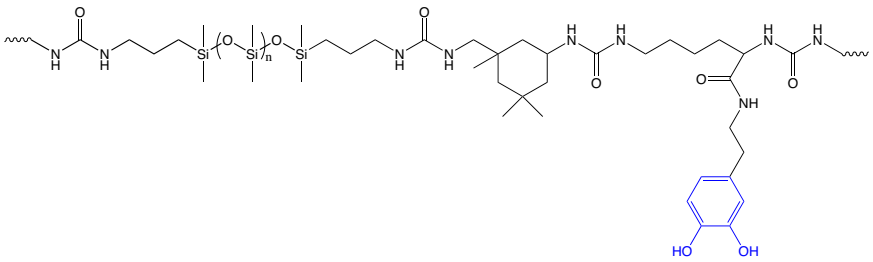

Fig. 1 Molecular structure of the intrinsic self-healing anticorrosion polymer (ISAP).

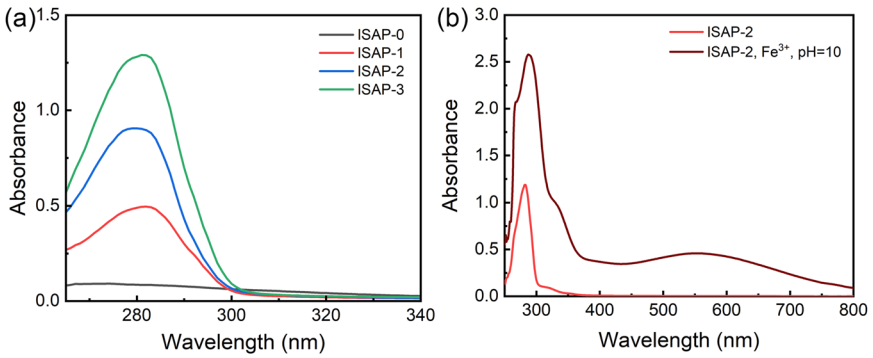

Fig. 2 The chemical component and coordination of the intrinsic self-healing anticorrosion polymers (ISAP) with Fe^{3+}. **a** Ultraviolet–visible (UV–vis) absorbance of the intrinsic self-healing anticorrosion polymers (ISAP), **b** UV–vis absorbance of the ISAP-2 and ISAP-2 with the addition of Fe^{3+} at pH = 10.

Table 1. Summary of the formula and molecular weight of intrinsic self-healing anticorrosion polymers (ISAP).

Sample	Molar ratio of PDMS: chain extender: IPDI	M_n ($\times 10^4$ g mol^{-1})	M_w ($\times 10^4$ g mol^{-1})	Polydispersity index (PDI)
ISAP-0	1:0:1	3.18	4.52	1.42
ISAP-1	1:0.1:1.1	2.48	4.48	1.80
ISAP-2	1:0.2:1.2	2.82	6.26	2.22
ISAP-3	1:0.3:1.3	2.64	5.78	2.19

Table 1 lists the compositions, molecular weights and polydispersity index (PDI) of the ISAP, where their chemical compositions were adjusted by varying the feeding ratios of PDMS, chain extender, and IPDI. Their molecular weights range from 2.48 to 3.18×10^4 g mol^{-1} and PDI range from 1.42 to 2.22. Their molecular structures were further confirmed by UV–vis and Fourier-transform infrared (FT-IR) spectroscopy (Fig. 2, Supplementary Figs. 5 and 6, Supplementary Table 1). In Fig. 2a, ISAP-0 shows a flat line with no absorption peaks, while the samples containing chain extender show absorption peaks at 285 nm, corresponding to the characteristic absorbance peak of catechol[44]. The intensity of the absorption peaks gradually increased with increasing chain extender content. These results indicate that the catechol group was successfully introduced into the polymer, and the group content was controllable. Furthermore, in Fig. 2b, an absorption peak between 500 and 700 nm is observed for ISAP-2 with added Fe^{3+} at pH of 10, which indicated the formation of a bis-/tris-complex.

Raman spectroscopy was performed to demonstrate the catechol-Fe^{3+} coordination. As shown in Fig. 3, a clear peak at 644 cm^{-1} was observed for ISAP-2, which represents the Fe–O bond vibrations of the catechol-metal complex[45,46]. In addition, resonance peaks at 1266, 1322, 1423, and 1428 cm^{-1} were observed, resulting from catechol ring vibrations, according to previous reports[45–47]. It clearly confirmed the polymer was able to form cross-links via the coordination of catechol with Fe^{3+}.

Mechanical property of the intrinsic self-healing anticorrosion polymers

The mechanical properties of the ISAP were further studied using tensile tests, the results for which are shown in Fig. 4. For ISAP-0, the tensile strength of the sample was 2.75 MPa, the Young's modulus was 4.12 MPa, and the toughness was 9.03 MJ cm^{-3}. With the increase in chain extender content, the tensile strength gradually increased from 3.25 to 5.16 MPa, and Young's modulus increased from 6.06 to 10.40 MPa. The toughness of ISAP-2 and ISAP-3 was comparable at ~11 MJ cm^{-3}, which is higher than that of ISAP-0. These results indicate that the introduced urea-hydrogen bonds and the rigid benzene ring structure in the polymer chain contribute to a gradual increase in the tensile strength, modulus, and toughness of the materials.

The self-healing properties of the ISAP samples were further investigated. Dumbbell-shaped specimens were cut off, realigned, and soaked in an $FeCl_3$ solution (0.01 mol L^{-1}) for different durations. As seen in Fig. 5, the stress-strain curve of ISAP-1 gradually coincided with that of the original sample, and the tensile strength was gradually restored with increasing immersion time. Additionally, the

self-healing efficiency of ISAP-0 was 45.9% after five days of immersion, while ISAP-1 reached as high as 67.9%. This is because the catechol group at the fracture interface of ISAP-1 was coordinated and crosslinked with Fe^{3+}, and the fracture interface was repaired. The above results indicate that the as-prepared ISAP samples can be repaired by the dynamic crosslinking of the polymer chains with Fe^{3+}.

Self-healing anticorrosion property of the polymer coating

The self-crosslinking of polymer chains with Fe^{3+} renders polymer application prospects for self-healing and anti-corrosion. We tested ISAP-0 and ISAP-2 polymer coatings on carbon steel. All the samples exhibited hydrophobicity with a water contact angle of ~105° and ~90° after immersion in 3.5 wt% NaCl solution for 2 months owing to the PDMS hydrophobic segments (Supplementary Figs. 6 and 7). This also indicated that the introduction of hydrophilic catechol did not change the surface properties of the coating.

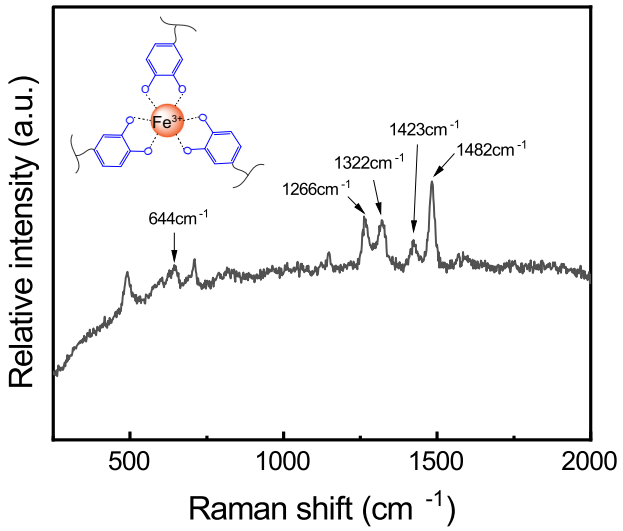

Fig. 3 The formation of catechol-Fe^{3+} coordination. The Raman spectra of the intrinsic self-healing anticorrosion polymers ISAP-2 with Fe^{3+} at pH = 10.

Salt immersion experiments were conducted to illustrate the self-healing anticorrosion properties of the ISAP coatings. Figure 6 shows the topographies of the scratched ISAP-0 and ISAP-2 coatings and the corresponding metal substrates after 7 days of immersion in salt water. For ISAP-0, the coating material exhibited severe scratch expansion and a large amount of metal rust was attached (Fig. 6a–c), indicating that severe corrosion occurred at scratches on the metal substrate. For ISAP-2, there were no noticeable changes in the polymer scratches, and the metal substrate was only slightly rusted (Fig. 6d–f). These results indicate that the ISAP-2 coating has a good self-healing anticorrosion effect.

The corrosion protection properties of the two coatings were further investigated using electrochemical impedance spectroscopy (EIS), of which results are shown in Fig. 7. The electrochemical impedance of the two coatings was tested by immersing them in a brine environment with NaCl (0.1 mol L^{-1} NaCl for 4, 24, 48, 72, and 96 h), and measurements were illustrated in Bode plots (Fig. 7a, b). For the scratched ISAP-0 coating, shown in Fig. 7a, the impedance values at low frequencies decreased rapidly after soaking for 4 to 48 h. In the Bode phase plots, with prolonged immersion time, two-time constants were clearly observed, which were related to the coating properties and the charge transfer process at the interface of metal and coating. These results suggest that the barrier properties of the scratched ISAP-0 coatings were severely deteriorated. For the ISAP-2 coating shown in Fig. 7b, the impedance values increased at both low and high frequencies after 24 h and 48 h of immersion. The impedance at low frequencies ($|Z|_{0.01\ Hz}$) is often used to semi-quantitatively describe the corrosion resistance of coatings. As

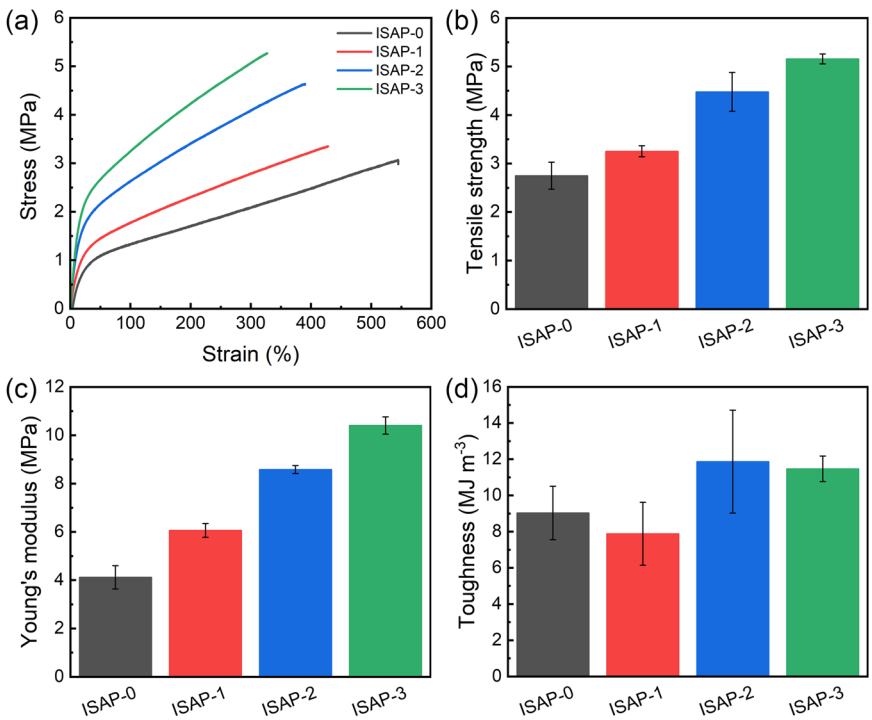

Fig. 4 Mechanical properties of the intrinsic self-healing anticorrosion polymers (ISAP). a Stress-strain curves, **b** tensile strength, **c** Young's modulus, and (**d**) toughness of the intrinsic self-healing anticorrosion polymers (ISAP) (error bars stand for the standard deviations from three independent samples).

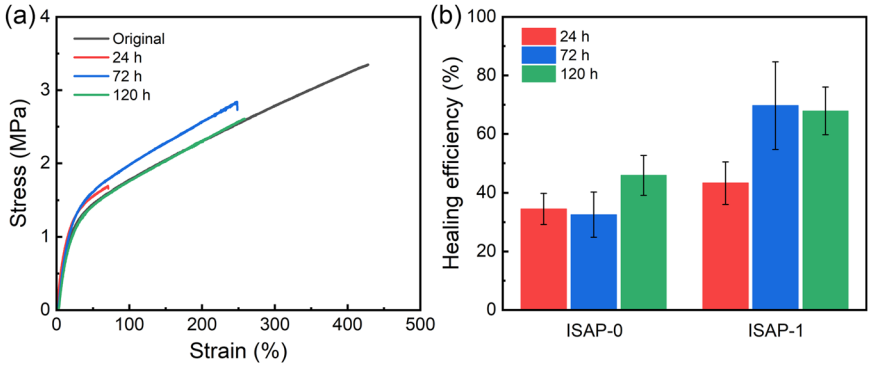

Fig. 5 The self-healing performance of the intrinsic self-healing anticorrosion polymers (ISAP). a Strain-stress curves of the original and self-healing ISAP-1 specimens after 24, 72, and 120 h immersed in an $FeCl_3$ solution (0.01 mol L^{-1}). **b** The self-healing efficiency of the ISAP-0 and ISAP-1 (error bars stand for the standard deviations from three independent samples).

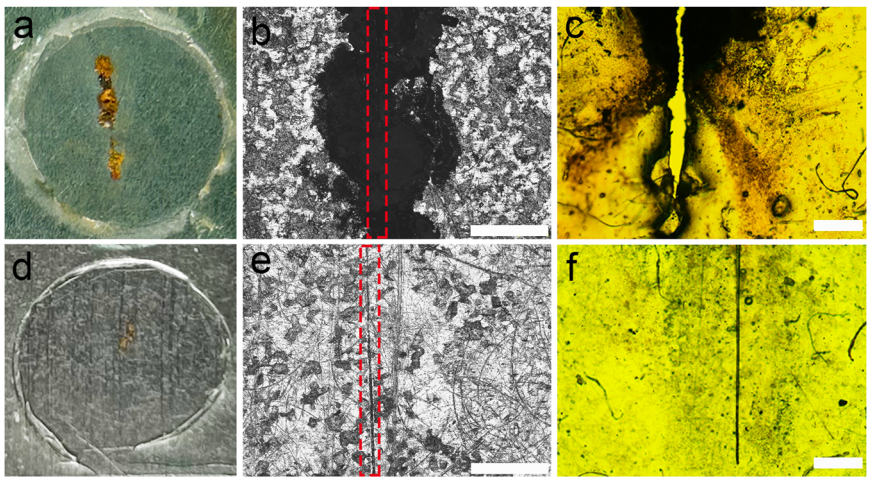

Fig. 6 The morphology of the scratched coatings after immersion in salt water. Photos (**a**, **d**) and Optical microscopy (**b**, **c**, **e**, **f**) of the scratched area after peeling coating from the metal substrates (**a**, **b**, **d**, **e**) and the peeled intrinsic self-healing anticorrosion polymer coating (**c**, **f**) after immersion in salt water (0.1 M) for 7 days. (**a**–**c**) ISAP-0, (**d**–**f**) ISAP-2. The length of the scratch: 0.5 cm. Scale bar: 500 μm.

shown in Fig. 7c, the $|Z|_{0.01\ Hz}$ value of ISAP-0 coating drops continuously from 3.58×10^4 to 0.93×10^4 ohm cm^2 in the extended immersion periods. For ISAP-2 coatings, the $|Z|_{0.01\ Hz}$ value was 2.35×10^4 ohm cm^2 at 4 h, 3.84×10^4 ohm cm^2 at 24 h and 7.29×10^4 ohm cm^2 at 48 h. After 96 h of immersion, the impedance value remained at a high value of 6.26×10^4 ohm cm^2 which is comparable to those of the intact ISAP-0 sample, even higher than that at 4 h (Fig. 7c and Supplementary Fig. 8). This indicates that the corrosion resistance of scratched ISAP-2 rapidly increases after soaking in salt-water. Therefore, the ISAP-2 coating exhibited self-healing anticorrosion performance.

Based on the above results, a self-healing anticorrosion mechanism for the ISAP-2 coating was proposed, as shown in Fig. 8. When the coating was damaged, corrosive media, such as water, O_2, and Cl^- penetrated the coating and a corrosion electrical reaction occurred on the metal substrate, leading to the production of Fe^{3+} and a weakly alkaline microenvironment as a result of the electrochemical corrosion process[48]. The polymer chains were self-crosslinked by the coordination of catechol and diffused Fe^{3+} ions in a weakly alkaline environment. The damaged area was further repaired, and the anticorrosion performance was recovered.

In summary, in-situ self-crosslinking strategy for constructing intrinsic self-healing anticorrosion polymers was demonstrated herein. Dynamic coordination crosslinks were formed between the catechol groups in the polymer chains and Fe^{3+} produced from the metal substrate. The as-synthesized polymers had tunable catechol content and good mechanical properties. In the presence of Fe^{3+}, the healing efficiency of the specimens obtained from the tensile stress was as high as 67.9%. Moreover, the prepared scratched polymer coating showed an increase of impedance values at 0.01 Hz from 2.35×10^4 ohm cm^2 at 4 h to 7.29×10^4 ohm cm^2 at 48 h according to the EIS experiments. This intrinsic self-healing anticorrosion polymer has potential applications in harsh environments.

METHODS

Materials

α,ω-Aminopropyl-terminated poly(dimethylsiloxane) (APT-PDMS) ($M_n = 2000$ g mol^{-1}) was purchased from Hangzhou Silong Mater. Tech. Co., Ltd. Isophorone diisocyanate (IPDI, 99%, Aladdin) was used as received. Superdry tetrahydrofuran (THF, 99.9%, J&K Scientific), superdry triethylamine (TEA, 99.5%, Meryer, China), and superdry *N*,*N*-dimethyl formamide (DMF, 99.8%, J&K Scientific) were used without further purification.

Synthesis of intrinsic self-healing anticorrosion polymers

Intrinsic self-healing anticorrosion polymers with different contents of chain extender were synthesized. The chain extender was synthesized according to a previous literature[43]. First, 0.978 g (4.4 mmol) of IPDI was placed in a three-necked

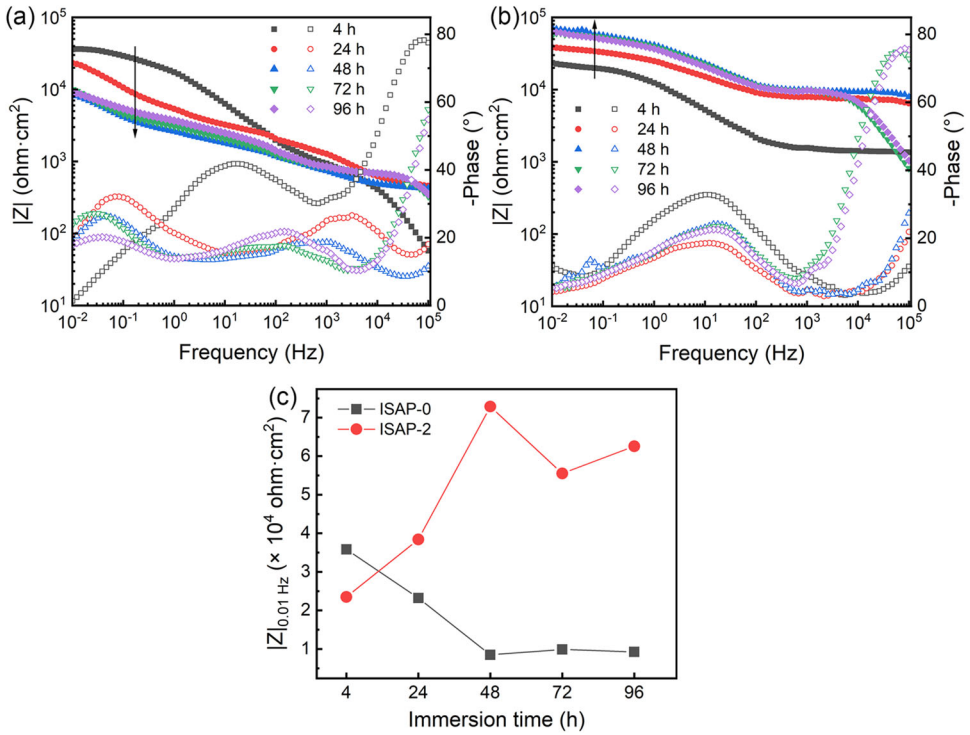

Fig. 7 The self-healing anticorrosion performance of the scratched intrinsic self-healing anticorrosion polymer (ISAP) coatings. EIS Bode plots of the scratched intrinsic self-healing anticorrosion polymer (ISAP) coatings ISAP-0 (**a**) and ISAP-2 (**b**) at different immersion times. Solid symbol represents |Z|. Hollow symbol represents -phase. **c** The impedance at low frequencies ($|Z|_{0.01\ Hz}$) of ISAP-0 and ISAP-2 with different immersion times.

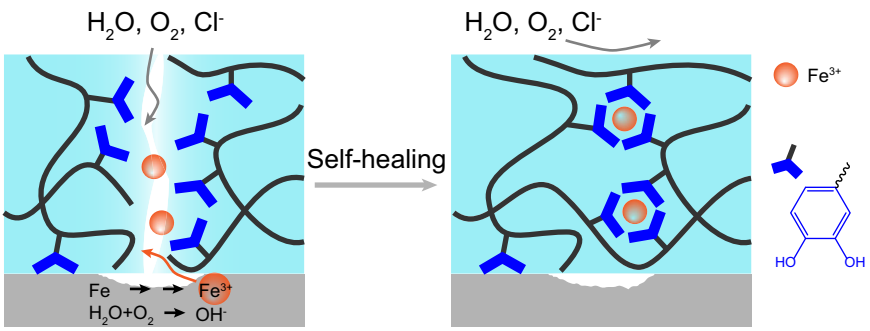

Fig. 8 Schematic of self-healing anticorrosion mechanism of the intrinsic self-healing anticorrosion polymer (ISAP) coating.

bottle under an Ar atmosphere. The as-synthesized chain extender (0.142 g, 0.4 mmol) was dissolved in the superdry DMF, followed by the addition of 0.081 g (0.8 mmol) of superdry TEA. The solution was then centrifuged. The supernatant was added dropwise to the IPDI and allowed to react for 4 h under Ar in an ice-water bath. APT-PDMS (8 g, 4 mmol) was heated at 120 °C for 2 h under vacuum to remove the moisture. The dried APT-PDMS was dissolved in 40 mL of superdry THF and added dropwise to the reaction solution. The mixture was allowed to react for 12 h under Ar at room temperature. The product was labeled ISAP-1.

Preparation of polymer anti-corrosion coatings

Carbon steel Q235 was used as the substrate for preparing the anticorrosion coating. Solutions containing 0.15 g ISAP-1 in 1.5 ml of THF were deposited onto clean carbon steel substrates. The coated samples were dried at room temperature for 24 h. The coating thickness was about 150 μm.

Characterization

The ^{1}H-NMR (600 MHz) spectra were recorded on a Bruker AVANCE III spectrometer using $CDCl_3$ and DMSO-d_6 as the solvents and tetramethylsilane (TMS) as the internal standard. Attenuated total reflection-Fourier-transform infrared (ATR-FTIR) spectra were obtained using a Thermo Scientific Nicolet 6700 spectrometer. The scanning range was 400–4000 cm^{-1}. The molecular weight and PDI were determined using a gel permeation chromatography (GPC) instrument (Waters 1515) with THF as the mobile phase. Ultraviolet−visible (UV−vis) absorption spectra were acquired using a Thermo Scientific Evolution 220 spectrophotometer at room temperature. Tensile tests were performed on a ZwickRoell instrument at a speed of 80 mm min^{-1} using a dumbbell-shaped sample. Three parallel samples of each polymer were tested. The water contact angle was measured using an OCA50 Dataphysics. Five different areas of each sample were tested and the average was calculated. Macroscopic healing tests of the coatings were conducted using an optical microscope (Axioskop40 A Pol, Nikon and Olympus BX53M). A scratch

(5 mm × 0.02 mm) was made on the coating using a cutter blade. The damaged coating was repaired by soaking in a 0.1 mol L^{-1} NaCl solution for 4, 24, 48, 72, and 96 h. Then, the polymer coating was peeled off from the metal substrate. EIS was conducted in a 0.1 mol L^{-1} NaCl solution using an electrochemical workstation (CHI 660E, Shanghai Chenhua Instrument Co., Ltd. China) with a frequency range from 10^5 to 10^{-2} Hz. A three-electrode system was used, consisting of a coated steel substrate as the working electrode, a saturated calomel electrode as the reference electrode, and a platinum foil as the counter electrode.

DATA AVAILABILITY

The data that support the findings of this study are available from the corresponding author upon reasonable request.

Received: 5 April 2023; Accepted: 23 July 2023;
Published online: 11 August 2023

REFERENCES

1. Diesendruck, C. E., Sottos, N. R., Moore, J. S. & White, S. R. Biomimetic self-healing. *Angew. Chem. Int. Ed.* **54**, 10428–10447 (2015).
2. Patrick, J. F., Robb, M. J., Sottos, N. R., Moore, J. S. & White, S. R. Polymers with autonomous life-cycle control. *Nature* **540**, 363–370 (2016).
3. Wang, S. & Urban, M. W. Self-healing polymers. *Nat. Rev. Mater.* **5**, 562–583 (2020).
4. Zhang, F. et al. Self-healing mechanisms in smart protective coatings: a review. *Corros. Sci.* **144**, 74–88 (2018).
5. Shchukin, D. & Mohwald, H. A coat of many functions. *Science* **341**, 1458–1459 (2013).
6. Lou, Y. et al. Microbiologically influenced corrosion inhibition of carbon steel via biomineralization induced by shewanella putrefaciens. *npj Mater. Degrad.* **5**, 59 (2021).
7. Udoh, I. I. et al. Active anticorrosion and self-healing coatings: a review with focus on multi-action smart coating strategies. *J. Mater. Sci. Technol.* **116**, 224–237 (2022).
8. García, S. J., Fischer, H. R. & van der Zwaag, S. A critical appraisal of the potential of self healing polymeric coatings. *Prog. Org. Coat.* **72**, 211–221 (2011).
9. Montemor, M. F. Functional and smart coatings for corrosion protection: a review of recent advances. *Surf. Coat. Technol.* **258**, 17–37 (2014).
10. Blaiszik, B. J. et al. Self-healing polymers and composites. *Annu. Rev. Mater. Res.* **40**, 179–211 (2010).
11. Saji, V. S. Organic nanotubes for smart anticorrosion and antibiofouling coatings. *npj Mater. Degrad.* **6**, 30 (2022).
12. Li, J., Shi, H., Liu, F. & Han, E.-H. Self-healing epoxy coating based on tung oil-containing microcapsules for corrosion protection. *Prog. Org. Coat.* **156**, 106236 (2021).
13. García, S. J. et al. Self-healing anticorrosive organic coating based on an encapsulated water reactive silyl ester: Synthesis and proof of concept. *Prog. Org. Coat.* **70**, 142–149 (2011).
14. Song, Y. et al. Synthesis of polyurethane/poly(urea-formaldehyde) double-shelled microcapsules for self-healing anticorrosion coatings. *Chin. J. Polym. Sci.* **38**, 45–52 (2020).
15. Caruso, M. M. et al. Robust, double-walled microcapsules for self-healing polymeric materials. *ACS Appl. Mater. Interfaces* **2**, 1195–1199 (2010).
16. Abdullayev, E., Price, R., Shchukin, D. & Lvov, Y. Halloysite tubes as nanocontainers for anticorrosion coating with benzotriazole. *ACS Appl. Mater. Interfaces* **1**, 1437–1443 (2009).
17. Shchukina, E., Grigoriev, D., Sviridova, T. & Shchukin, D. Comparative study of the effect of halloysite nanocontainers on autonomic corrosion protection of polyepoxy coatings on steel by salt-spray tests. *Prog. Org. Coat.* **108**, 84–89 (2017).
18. Shchukina, E., Shchukin, D. & Grigoriev, D. Halloysites and mesoporous silica as inhibitor nanocontainers for feedback active powder coatings. *Prog. Org. Coat.* **123**, 384–389 (2018).
19. Ma, Y. Q. et al. Superior anti-corrosion and self-healing bi-functional polymer composite coatings with polydopamine modified mesoporous silica/graphene oxide. *J. Mater. Sci. Technol.* **95**, 95–104 (2021).
20. Wang, T., Du, J., Ye, S., Tan, L. H. & Fu, J. J. Triple-stimuli-responsive smart nanocontainers enhanced self-healing anticorrosion coatings for protection of aluminum alloy. *ACS Appl. Mater. Interfaces* **11**, 4425–4438 (2019).
21. Zhou, C. L. et al. Metal organic frameworks (MOFs) as multifunctional nanoplatform for anticorrosion surfaces and coatings. *Adv. Colloid Interface Sci.* **305**, 102707 (2022).
22. Yang, S. et al. pH-responsive zeolitic imidazole framework nanoparticles with high active inhibitor content for self-healing anticorrosion coatings. *Colloids Surf. A Physicochem. Eng. Asp.* **555**, 18–26 (2018).
23. Wang, J.-P. et al. Adaptive polymeric coatings with self-reporting and self-healing dual functions from porous core–shell nanostructures. *Macromol. Mater. Eng.* **303**, 1700616 (2018).
24. Li, G. L., Schenderlein, M., Men, Y., Möhwald, H. & Shchukin, D. G. Monodisperse polymeric core–shell nanocontainers for organic self-healing anticorrosion coatings. *Adv. Mater. Interfaces* **1**, 1300019 (2014).
25. Li, C., Guo, X. & Frankel, G. S. Smart coating with dual-pH sensitive, inhibitor-loaded nanofibers for corrosion protection. *npj Mater. Degrad.* **5**, 54 (2021).
26. Chen, Z., Scharnagl, N., Zheludkevich, M. L., Ying, H. & Yang, W. Micro/nano-container-based intelligent coatings: synthesis, performance and applications – a review. *Chem. Eng. J.* **451**, 138582 (2023).
27. Fu, X. et al. Nanofiber composite coating with self-healing and active anticorrosive performances. *ACS Appl. Mater. Interfaces* **13**, 57880–57892 (2021).
28. Thongchaivetcharat, K., Salaluk, S., Crespy, D., Thérien-Aubin, H. & Landfester, K. Responsive colloidosomes with triple function for anticorrosion. *ACS Appl. Mater. Interfaces* **12**, 42129–42139 (2020).
29. Li, B., Xue, S., Mu, P. & Li, J. Robust self-healing graphene oxide-based superhydrophobic coatings for efficient corrosion protection of magnesium alloys. *ACS Appl. Mater. Interfaces* **14**, 30192–30204 (2022).
30. Cheng, L., Liu, C. B., Zhao, H. C. & Wang, L. P. Photothermal-triggered shape memory coatings with active repairing and corrosion sensing properties. *J. Mater. Chem. A* **9**, 22509–22521 (2021).
31. Li, Y. et al. Application of hierarchical bonds for construction an anti-corrosion coating with superior intrinsic self-healing function. *Colloids Surf. A Physicochem. Eng. Asp.* **639**, 128388 (2022).
32. Huang, Y. et al. Triple-action self-healing protective coatings based on shape memory polymers containing dual-function microspheres. *ACS Appl. Mater. Interfaces* **10**, 23369–23379 (2018).
33. Liu, C., Wu, H., Qiang, Y., Zhao, H. & Wang, L. Design of smart protective coatings with autonomous self-healing and early corrosion reporting properties. *Corros. Sci.* **184**, 109355 (2021).
34. Liu, T. et al. Ultrafast and high-efficient self-healing epoxy coatings with active multiple hydrogen bonds for corrosion protection. *Corros. Sci.* **187**, 109485 (2021).
35. Auepattana-Aumrung, K. & Crespy, D. Self-healing and anticorrosion coatings based on responsive polymers with metal coordination bonds. *Chem. Eng. J.* **452**, 139055 (2023).
36. Yang, Y. F., Ren, J. Y., Luo, C. X., Yuan, R. Q. & Ge, L. Q. Fabrication of l-menthol contained edible self-healing coating based on guest-host interaction. *Colloids Surf. A Physicochem. Eng. Asp.* **597**, 124743 (2020).
37. Wu, B., Yuan, A., Xiao, Y., Wang, Y. & Lei, J. Study on a polyacrylate-based waterborne coating: facile preparation, convenient self-healing behavior and photoluminescence properties. *J. Mater. Chem. C* **8**, 12638–12647 (2020).
38. Li, X. et al. Bio-inspired self-healing mxene/polyurethane coating with superior active/passive anticorrosion performance for mg alloy. *Chem. Eng. J.* **454**, 140187 (2023).
39. Zou, Y. et al. Silane modified epoxy coatings with low surface tension to achieve self-healing of wide damages. *Prog. Org. Coat.* **133**, 357–367 (2019).
40. Khan, A., Huang, K., Sarwar, M. G. & Rabnawaz, M. High modulus, fluorine-free self-healing anti-smudge coatings. *Prog. Org. Coat.* **145**, 105703 (2020).
41. Ekeocha, J. et al. Challenges and opportunities of self-healing polymers and devices for extreme and hostile environments. *Adv. Mater.* **33**, e2008052 (2021).
42. Aguirresarobe, R. H. et al. Healable and self-healing polyurethanes using dynamic chemistry. *Prog. Polym. Sci.* **114**, 101362 (2021).
43. Sun, P. et al. Facile and universal immobilization of l-lysine inspired by mussels. *J. Mater. Chem.* **22**, 10035–10041 (2012).
44. Black, K. C. L., Liu, Z. & Messersmith, P. B. Catechol redox induced formation of metal core-polymer shell nanoparticles. *Chem. Mater.* **23**, 1130–1135 (2011).
45. Holten-Andersen, N. et al. pH-induced metal-ligand cross-links inspired by mussel yield self-healing polymer networks with near-covalent elastic moduli. *Proc. Natl. Acad. Sci. USA* **108**, 2651–2655 (2011).
46. Harrington, M. J., Masic, A., Holten-Andersen, N., Waite, J. H. & Fratzl, P. Iron-clad fibers: a metal-based biological strategy for hard flexible coatings. *Science* **328**, 216–220 (2010).
47. Hwang, D. S. et al. Protein- and metal-dependent interactions of a prominent protein in mussel adhesive plaques. *J. Biol. Chem.* **285**, 25850–25858 (2010).
48. Maile, F. J., Schauer, T. & Eisenbach, C. D. Evaluation of corrosion and protection of coated metals with local ion concentration technique (lict). *Prog. Org. Coat.* **38**, 111–116 (2000).

ACKNOWLEDGEMENTS

This work was funded by National Natural Science Foundation of China (Grant No.21975261 and No.22275012) and Fundamental Research Funds for the Central Universities (buctrc202125, buctrc202126).

AUTHOR CONTRIBUTIONS

Y.S.-Experimental design, data acquisition and analysis, manuscript writing and editing; A.K.-Data collection; D.C.-Data collection; G.L.L.-Conceptualization, supervision, writing review and editing. All authors discussed the results and contributed to the final version of the manuscript.

COMPETING INTERESTS

The authors declare no competing interests.

ADDITIONAL INFORMATION

Supplementary information The online version contains supplementary material available at https://doi.org/10.1038/s41529-023-00381-2.

Correspondence and requests for materials should be addressed to Guo Liang Li.